HTML ABSTRACT + LINKS

Edge rotation and temperature diagnostic on the National Spherical Torus Experiment

T. M. Biewer,[a] R. E. Bell, R. Feder, D. W. Johnson, and R. W. Palladino
Princeton Plasma Physics Laboratory, Princeton, New Jersey 08543

(Received 27 August 2003; accepted 4 December 2003)

A new diagnostic for the National Spherical Torus Experiment is described whose function is to measure ion rotation and temperature at the plasma edge. The diagnostic is sensitive to C III, C IV, and He II intrinsic emission, covering a radial region of 15 cm at the extreme edge of the outboard midplane. Thirteen chords are distributed between toroidal and poloidal views, allowing the toroidal and poloidal rotation and temperature of the plasma edge to be simultaneously measured with 10 ms resolution. Combined with the local pressure gradient and EFIT reconstructed magnetic field profile, the edge flow gives a measure of the local radial electric field. © *2004 American Institute of Physics.* [DOI: 10.1063/1.1646740]

I. INTRODUCTION

Plasma rotation has been theoretically and experimentally linked with improved stability and confinement.[1,2] In particular, sufficient flow shear in the plasma edge is expected to suppress turbulent eddies and induce a transition from low- to high-confinement mode (L mode–H mode) as is observed in traditional tokamak magnetic confinement devices, such as DIII–D[3] and JET,[4] and in spherical tokamaks[5] such as MAST[6] and the National Spherical Torus Experiment (NSTX).[7] It is believed that increased plasma flow is correlated with an increased radial electric field in the edge, leading to the L–H transition.[8] The radial electric field can be calculated from force balance, assuming that the toroidal and poloidal components of the plasma flow are measured, along with the magnetic field components and the plasma pressure. In this article a new diagnostic is presented which measures the poloidal and toroidal flow velocities and temperatures in the edge of NSTX plasmas.

The intrinsic emission of edge ions can be extremely bright, and hence, easily accessible as a plasma diagnostic. The intrinsic emission of C III impurity light, for example, rivals the brightness of the D_α emission from deuterium fueled NSTX plasmas. Together, the emission from these lines constitutes the majority of visible light that is observable from typical NSTX discharges. Carbon is the main impurity in NSTX due to the presence of protective carbon tiles throughout the machine. Light is emitted by excited ions at the edge of the plasma primarily from electron impact ionization. Due to the presence of a steep electron temperature gradient at the edge, narrow shells of intrinsic emission are formed at the edge of the plasma. The intersection of a diagnostic sightline with an edge intrinsic emission shell gives a spatial localization to the spectroscopic measurement. Multiple sightlines tangent to the flux surfaces accommodate various plasma sizes, and with enough resolution can be inverted to give local measurements and gradients.[9–11]

Because the intrinsic emission of the ions is used, active techniques to stimulate emission (e.g., neutral particle beams) are not necessary, allowing measurements to be made in essentially all types of NSTX plasma discharges. Since this edge rotation diagnostic (ERD) and the charge exchange recombination spectroscopy (CHERS)[12] diagnostic both measure the spectra of impurity ions, the techniques compliment each other, although CHERS measurements are limited to plasmas with neutral beam injected (NBI) power.

Since more than one spectral line is observed with the ERD, it is possible to make simultaneous measurements of multiple ion species, in multiple charge states, and at multiple locations in the plasma. The diagnostic described here is sensitive to light from C III, C IV, and He II intrinsic emission.

II. THE LIGHT DETECTION SYSTEM

Light is collected from multiple sightlines through the plasma, as shown in Figs. 1 and 2, and focused onto a single charge coupled device (CCD) camera, after dispersion by a single spectrometer. Using a single spectrometer and CCD detector to image both poloidal and toroidal views saves cost and reduces systematic errors by simplifying calibration.

The collection optics are rigidly mounted outside of the vacuum vessel. The plasma is viewed poloidally through a 20 cm vacuum window on the top of the machine at Bay B, which is located above a 5 cm gap in the NSTX passive stabilizing plates. Toroidally, the plasma is viewed through a 10 cm vacuum window off the pumping duct at the midplane of Bay L, which is shared by the CHERS background viewing optics. The CHERS background sightlines view toroidally at the midplane of the plasma, and the ERD sightlines are parallel to them, but displaced vertically downward by ~2–3 cm at the radii of tangency. Shutters are mounted on the vacuum side of both windows for protection during vacuum vessel bakeout and He glow-discharge cleaning.

There are six poloidal and seven toroidal sightlines, which utilize essentially identical optical systems to measure the light from intrinsic emission of the plasma. For the po-

[a]Electronic mail: tbiewer@pppl.gov

 © 2004 American Institute of Physics

Downloaded 22 Mar 2004 to 198.35.3.213. Redistribution subject to AIP license or copyright, see http://rsi.aip.org/rsi/copyright.jsp

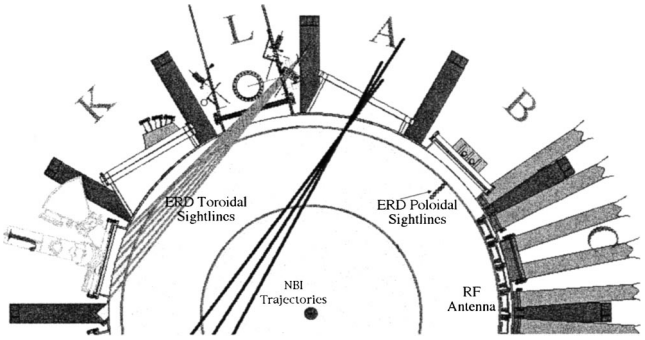

FIG. 1. Toroidal cross section of the NSTX vacuum vessel showing the toroidal ERD sightlines.

loidal sightlines, six fiber optics are held in a precisely machined mount at a fixed distance from a collection lens, and with an angular separation between fibers about the optical axis of the lens. This arrangement results in a fan of sightlines from the collection lens through the plasma. In the poloidal direction these sightlines are focused approximately 1.7 m from the collection lens, i.e., approximately on the midplane of the plasma. The images of the 600 μm diameter fibers are ~1.5 cm in diameter and spaced 3–4 cm apart on the midplane. In the toroidal direction, the sightlines are focused 1.7 m from the collection lens, i.e., at the point of tangency of the sightline to the plasma. The sightlines are parallel by design to the outermost sightlines of the CHERS background diagnostic, and utilize the same collection lens.

The light is collected from the plasma with two standard camera lenses (one toroidally and one poloidally viewing) of nominal 85 mm focal length at $f/1.8$. These lenses are identical to the spectrometer input lens, giving optimal coupling between the collected plasma light and the spectrometer. The

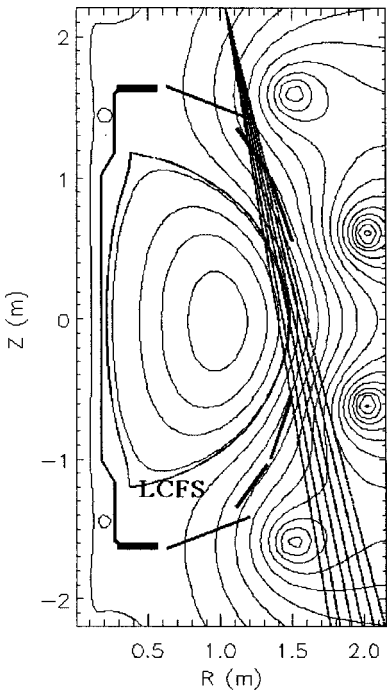

FIG. 2. Poloidal cross section of the NSTX vacuum vessel showing the EFIT reconstruction of Shot 110077 at 313 ms and the poloidal ERD sightlines.

light is imaged from the plasma onto fiber optics, which carry the light from the NSTX machine area into an adjacent room, where the detection hardware is located. The output end of the 13 fibers are held vertically in a single column in front of the spectrometer entrance slit by a precisely machined mount.

The spectrometer is commercially available from Kaiser Optical Systems, Inc.[13] It is a modified Holospec model HS-f/2.2-VIS, and uses a standard camera lens with a focal length of 85 mm at $f/1.8$ to image the entrance slit. Light is focused through a high dispersion, holographic transmission grating that is sandwiched between two prisms. The center wavelength of the grating was selected to be 4650 Å, i.e., near the C III triplet. A 58 mm focal length output lens at $f/1.2$ has been substituted for the standard output lens. This lens arrangement demagnifies the image while preserving the etendue of the system.

Because of the short focal length of the spectrometer, there is a strong curvature of the image plane unless a curved entrance slit is used. A linear entrance slit would result in a strongly curved image. Hence, by imposing compensating curvature of the proper radius on the entrance slit, the image can be made linear. This effect is described in detail in Ref. 14. The fiber holder was machined such that the fibers describe an arc with a radius of curvature of 39.22 mm. This curvature is likewise imposed on the entrance slit of the spectrometer, which has a slit width of 75 μm and a linear height of 11.3 mm. The entrance slits were custom made by Lenox Laser.[15] The diagnostic described here differs from that in Ref. 14 in that the ERD uses curved entrance slits (to produce a straight image), it operates at a different wavelength range and at higher dispersion, and it relies on intrinsic emission of light rather than neutral beam excited charge exchange emission (which allows the ERD to collect data in a wider range of experiments).

The CCD detector was once commercially available from Roper Scientific[16] (model Pentamax), and has a 512 $\times$512 array of 15$\times$15 μm pixels, for an active area of 7.68 $\times$7.68 mm. The well depth of each pixel is 10^5 electrons. The detector is thinned and backilluminated, with a quantum efficiency of 68% at 4650 Å. The camera can read out at 5 MHz, with 12 bit resolution. With on-chip binning (47 bins), a single frame can be read out in 10 ms. The camera is run by a dedicated PC, which is controlled by internal macrocommands and external triggers, communicated via FTP. A two-tab optical chopper wheel rotating at 50 Hz with a Scitec Instruments[17] chopper controler is used to shade the CCD during frame transfer, preventing image smearing. Without the chopper, light falling on the face of the CCD during frame readout would result in extraneous photoelectrons from bright lines accumulating in other pixels as the data are shifted out, across the CCD into the shift register. This effect is particularly important in CCD cameras which have comparable integration and shift times. To accommodate the chopper between the spectrometer and camera bodies, it was necessary to replace the standard 4 in. chopper wheel with a balanced 6 in. wheel. The chopper is synchronized at 100 Hz to the NSTX master clock before the start of the discharge, along with the camera readout timing.

Downloaded 22 Mar 2004 to 198.35.3.213. Redistribution subject to AIP license or copyright, see http://rsi.aip.org/rsi/copyright.jsp

III. RESULTS

A. Calibration

Calibration of the ERD system requires multiple steps. The CCD camera must be aligned with the spectrometer. The spatial locations of the diagnostic sightlines must be measured. The channel-to-channel sensitivity of the sightlines must be taken into account. Finally, the spectral mapping of the CCD must be carefully calibrated.

The alignment of the CCD detector plane to the exit focal plane of the spectrometer is accomplished by micrometer adjustments to commercially available translation and rotation stages affixed to the spectrometer and camera bodies, which give six degrees-of-adjustment (three translational and three rotational). This alignment was carried out with an illuminated slit before the fiber optics were attached to the spectrometer. A spare fiber mount was populated with two test fibers, and attached to the spectrometer. Filling these test fibers with white light yields two nominally horizontal bars of light on the detector. The rotation of the camera with respect to the spectrometer was adjusted until the two lines of white light were alligned with the CCD rows. Replacing the white light source with a neon gas filled, copper hollow-cathode lamp, gives a spectrum of lines, which can be used to adjust the translational and other rotational degrees of freedom. The width of the bright Cu 4651 Å line was used to adjust the focus of the spectrometer. Fine adjustments to these settings were later made after the fiber optic bundle was attached to the spectrometer, using the copper hollow-cathode lamp to fill the input end of the fibers. A neon pen-lamp was occasionally used throughout this process, in place of the Cu hollow-cathode lamp. There are many neon lines within the spectral range of this spectrometer, which were helpful in checking the alignment of different regions of the CCD detector, though the neon lines are considerably weaker than the Cu 4651 Å line.

The spatial locations of the diagnostic sightlines were found through an in-vessel calibration process with backlit fibers. A bright, white light source was projected onto the output end of the fibers. By placing a screen inside the vacuum vessel, the projection of light indicated where each fiber was viewing. The position of the backlit spot was measured at multiple positions along the sightline (by moving the screen), with respect to the wall of the vessel through the use of a calibrated FARO measurement arm.[18] Fitting a line through the spot locations of each fiber, gave an accurate measure of the sightline path. This was done for both the poloidal and toroidal views. While the FARO arm is reliably accurate to less than 0.1 mm, and locating the backlit fiber centers relative to each other is very precise, locating the centers relative to the vacuum vessel is less precise. Comparisons from successive calibrations suggest that the spatial calibration of the sightline is accurate to $\sim$1.5 mm.

After the fibers were attached to the spectrometer, spectral calibrations could be completed with the entire optical system in its final configuration. Minor adjustments to the camera/spectrometer orientation were made, as discussed earlier. Then, from inside the vacuum vessel, an extended, uniform white light source was used to fill the collection optics of first the poloidal, then the toroidal views. This provided a channel-to-channel, relative sensitivity calibration of the detector, which is referred to as a ''white plate'' calibration. The white plate was crosscalibrated with a Labsphere[19] blackbody source to get an absolute intensity calibration. The Labsphere could not be used to directly calibrate each channel due to physical interference between the Labsphere body and internal NSTX structures.

It is important when measuring the instrument transfer function to fill the optics in the same manner as for the experimental measurements. The preferred technique was to use the light emitted by a vessel-filling, neon glow discharge. This method has the advantage that the calibration is performed with light that is gathered along the exact sightlines of the diagnostic that measurements of rotation and temperature are made during plasma shots. A parallel technique done in vessel uses the copper hollow cathode lamp with a collimating lens to individually fill each fiber. The Cu 4651 Å line and minor neon lines were used to get the spectral calibration of each detector channel. The dispersion of the system is roughly 0.222 Å/pixel, though it varies somewhat across the CCD. The instrumental temperature is $\sim$40 eV, which corresponds to an instrumental width of $\sim$2.9 pixels.

B. Operation

Since this was a new, prototype diagnostic, some adjustments to the diagnostic were necessary once initial measurements were made. In the original configuration the ERD suffered from saturated channels. Adding additional CCD readout bins (i.e., less light per bin) to the brightest sightlines, mitigated some of the problem. Maintaining a 10 ms frame rate imposed a 47 bin maximum. The aperture of the spectrometer entrance lens had to be decreased to limit the light intensity on the CCD. Ultimately, an aperture of $f/11$ was deemed necessary, which collects only 2.7% of the light available at $f/1.8$. Even at this reduced aperture, the ERD measures $>10^5$ photoelectrons of C III light in 10 ms for a given sightline during typical operating conditions. The light collection system described here was originally designed for the poloidal rotation system on the tokamak fusion test reactor,[14] which required high throughput, and was later adapted for use on NSTX. Clearly, the present application would benefit greatly from a faster CCD camera, allowing higher time resolution data to be measured without sacrificing the present signal-to-noise ratio (by opening the aperture).

C. Experimental data

The NSTX is a large spherical tokamak with a major radius of 0.85 m and a minor radius of 0.65 m. The plasma poloidal cross section is strongly shaped with high vertical elongation, as can be seen in Fig. 2. Typical pulse lengths of NSTX discharges are $\simeq$1 s, with an on-axis toroidal magnetic field between 0.3 and 0.6 T. The plasma current is typically $\leqslant$1.5 MA.

Figure 3 shows sample spectra from two NSTX discharges. A full frame of data covers the wavelength range from 4595 to 4705 Å. Partial spectra are shown here to high-

Downloaded 22 Mar 2004 to 198.35.3.213. Redistribution subject to AIP license or copyright, see http://rsi.aip.org/rsi/copyright.jsp

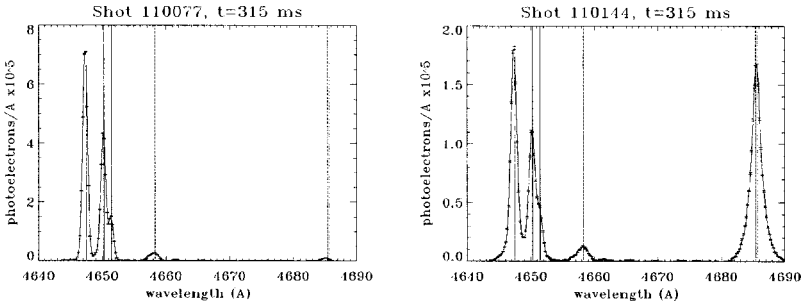

FIG. 3. Sample spectra from (a) Shot 110077 (NBI heated D_2 plasma) and (b) Shot 110144 (radio frequency heated He plasma). The nonshifted line centers are represented by the vertical solid lines (C III), dashed lines (C IV), and dotted line (He II). Error bars indicate the statistical uncertainty in the data.

light the C III, C IV, and He II lines. The error bars represent the statistical error in the data. The error is small, due to the large number of detected photons. The C III triplet (4647.419, 4650.246, and 4651.473 Å) is from the ^3S to $^3P_0$ transition.[20] The relative amplitude and wavelengths of the three lines are well known.[21] Each of the lines is from the same lower energy state, and the upper energy state should be statistically populated. Hence, any amplitude variation depends not on plasma parameters but on the $(2J+1)$-sum rule of the upper energy state.[22] The line intensity ratios measured here are in agreement with the published ratios. A three Gaussian fit to the data is constrained by the relative amplitudes and the fixed relative separations of the three spectral lines. Thus, the three free parameters which are fit to the data are the overall amplitude, the line shift of the triplet (the plasma velocity), and a single linewidth (the ion temperature). Fitting to all three lines simultaneously not only increases the amount of signal utilized, but also improves the robustness of the fit, since parasitic lines (i.e., non C III) within the fit range are unlikely to affect the fit.

Each sightline gives a line-averaged measure of the intrinsic emission of a given species in the edge of the plasma. By inverting the data, a local measure of the ion spectral line emissivity, velocity, and temperature can be found. Figure 4(a) shows typical edge profiles of the C III brightness as measured by the toroidal and poloidal views during Shot 110077. These data can be inverted to give the local emissivity of the C III shell,[9–11] as shown in Fig. 4(b). In the toroidal view, the radii listed are the tangency radii of the sightlines. Since the poloidal cross section is noncircular, the radii listed for the poloidal view are the midplane radii of the flux surface where each sightline is tangent (above the midplane.) Also shown in Fig. 4 is the radial location of the last closed flux surface (LCFS) as calculated from the EFIT equilibrium reconstruction,[23] which occurs just outside the peak in the C III emission. The agreement between the toroidal and poloidal views (which are toroidally separated by 90°) in the amplitude and location of the emission shell is indicative that the intrinsic emission is isotropic on the flux surfaces.

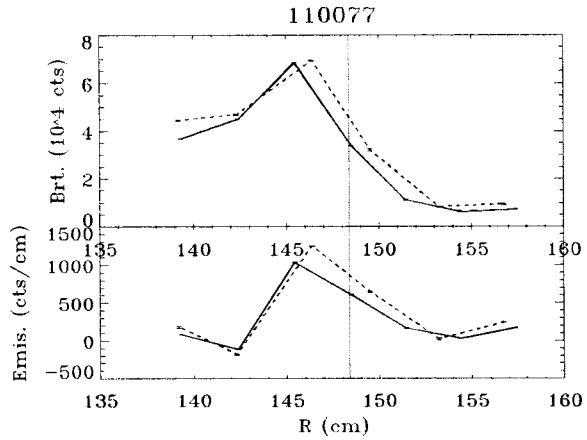

FIG. 4. Edge profiles of C III (a) brightness and (b) emissivity from the poloidal (dashed) and toroidal (solid) views at 315 ms in Shot 110077.

The radial width of the emission shell in this discharge is on the order of the sightline separation. Hence, the edge ion velocity (and temperature) can only be measured for C III at one (or possibly two) radial locations. Observations show that the radius of peak emissivity evolves during discharges over the radial range of the diagnostic. Thus, while the radial coverage of the ERD appears apt for a measurement of the local velocity (and, hence, radial electric field), the radial resolution may be inadequate to measure gradients in these quantities for a single charge state in a discharge with a steep electron temperature gradient. The radial resolution of the ERD could be improved by replacing the 600 μm diameter fibers with a more closely spaced array of 200 μm diameter fibers. This factor of 10 reduction in gathered light could easily be countered by increasing the aperture of the optics from $f/11$.

Shot 110077 is a double-null, D_2 fueled discharge, with a plasma current of 1 MA, on-axis toroidal magnetic field of 0.45 T, and up to 5.1 MW of NBI power. The discharge transits into ''high confinement mode,'' or *H*-mode beginning around 240 ms and lasts for roughly 250 ms, until the discharge terminates. During the *H*-mode period, there are multiple bursts of edge-localized modes (ELMs), indicated by spikes in the D_α trace shown in Fig. 5(a). A closer inspection reveals that there are also ELM-free *H*-mode periods, e.g., from 230 to 250 ms, and from 305 to 330 ms. The NBI power is increased stepwise by 1.7 MW at 60, 160, and 320 ms from 0 to 5.1 MW. Figure 5(b) shows the time evolution of the radii of peak toroidal and poloidal C III emission as the discharge progresses, along with the EFIT calculated location of the LCFS. Figures 5(c) and 5(d) show the time evolution of the apparent temperature and local velocity, respectively, for both the toroidal and poloidal views at the radii of maximum emissivity. The error bars in the plots are indicative of the propagated statistical error of the measurement. Toroidally, a positive velocity is in the direction of the plasma current and the neutral beams. Poloidally, a positive velocity is downward on the outboard side of the machine.

The poloidally and toroidally measured temperatures in Fig. 5(c) appear unequal at times in the discharge. Close

Downloaded 22 Mar 2004 to 198.35.3.213. Redistribution subject to AIP license or copyright, see http://rsi.aip.org/rsi/copyright.jsp

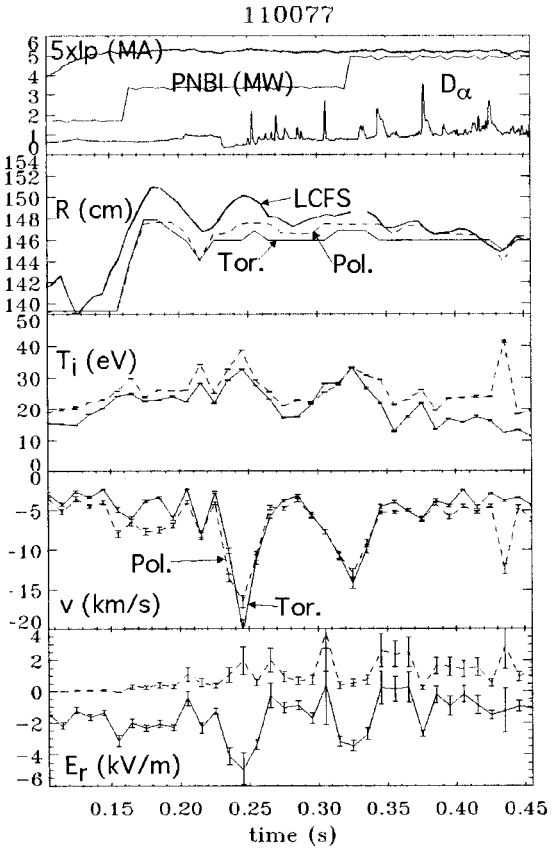

FIG. 5. Sample data during Shot 110077, showing (a) the plasma current, neutral beam injected power, and a D_α trace, and from the C III lines (solid =toroidal, dashed=poloidal), (b) radii of peak emissivity compared to EFIT calculated LCFS (heavy solid), (c) the apparent temperature at the earlier radii, (d) and the local rotation velocity, and (e) $E_r=-(\mathbf{v}\times\mathbf{B})_r+\nabla p/Zen$ (solid line) from the earlier measurements. The $\nabla p/Zen$ (dashed line) contribution is also plotted separately.

inspection of Fig. 5(b) shows that the radial location of the two temperatures shown is slightly different. This is one possible source of the apparent anisotropy, since in *H*-mode plasmas the edge temperature gradient can be very steep. The radial difference between the poloidal and toroidal views is a consequence of the fact that the emission shell width is comparable to the chordal spacing of the diagnostic. Moreover, the error bars given are representative of the statistical error of the measurement, but do not include a systematic error estimate. With these caveats, the apparent anisotropy can be interpreted as an upper limit to the nonstatistical limitation of the diagnostic, with its present spatial resolution.

From force balance $E_r=-(\mathbf{v}\times\mathbf{B})_r+\nabla p/Zen$, for each species. Figure 5(e) shows the calculation of the radial electric field, E_r. The radial $-\mathbf{v}\times\mathbf{B}$ terms, are calculated from these measurements and the EFIT reconstruction of the magnetic field, **B**. The $\nabla p/Zen$ term is also calculated. In this term T_i is measured by the ERD, and n_i is calculated from the measured emissivity profiles using photoemission coefficients from ADAS[24] modeling with the Thomson scattering measured T_e and n_e values.

ACKNOWLEDGMENTS

The authors wish to recognize the many contributions of the NSTX group, particularly Steve Sabbagh for providing the EFIT reconstructions, Vlad Soukhanovskii for the ADAS computations, and Benoit LeBlanc for the TS measurements. This research was supported by the U.S. D.O.E. under Contract No. DE-AC02-76CH03073.

[1] P. W. Terry, Rev. Mod. Phys. **72**, 109 (2000).
[2] H. Biglari, P. Diamond, and P. Terry, Phys. Fluids B **2**, 1 (1990).
[3] T. N. Carlstrom, R. J. Groebner, C. Fenzi, G. R. McKee, R. A. Moyer, and T. L. Rhodes, Plasma Phys. Controlled Fusion **44**, 333 (2002).
[4] A. Gibson, Phys. Plasmas **5**, 1839 (1998).
[5] Y.-K. Peng and D. Strickler, Nucl. Fusion **26**, 769 (1986).
[6] A. Sykes *et al.*, Phys. Plasmas **8**, 2101 (2001).
[7] J. Spitzer *et al.*, Fusion Technol. **30**, 1337 (1996).
[8] R. J. Akers *et al.*, Phys. Rev. Lett. **88**, 035002 (2002).
[9] R. E. Bell, Rev. Sci. Instrum. **66**, 558 (1994).
[10] R. E. Bell, Rev. Sci. Instrum. **68**, 1273 (1996).
[11] I. Condrea, E. Haddad, B. C. Gregory, and G. Abel, Phys. Plasmas **7**, 3641 (2000).
[12] B. Stratton, R. J. Fonk, K. P. Jaehnig, N. Schechtman, and E. J. Synakowski, in *Proceedings of the IAEA Technical Committee Meeting on Time Resolved Two- and Three-Dimensional Plasma Diagnostics, Najoya, Japan, 1990* (IAEA, Vienna, 1991), p. 78.
[13] Kaiser Optical Systems, Inc., Ann Arbor, MI, http://www.kosi.com.
[14] R. E. Bell, L. E. Dudek, B. Grek, D. W. Johnson, and R. W. Palladino, Rev. Sci. Instrum. **70**, 821 (1998).
[15] Lenox Laser, Inc., Glen Arm, MD, http://www.lenoxlaser.com.
[16] Roper Scientific, Inc., Trenton, NJ, http://www.roperscientific.com.
[17] Scitec Instruments, Ltd., Cornwall, England, http://www.scitec.uk.com.
[18] FARO Technologies, Inc., Lake Mary, FL, http://www.faro.com.
[19] Labsphere Inc., Sutton, NH, http://www.labsphere.com.
[20] A. R. Striganov and N. S. Sventitskii, *Tables of Spectral Lines of Neutral and Ionized Atoms* (Plenum, New York, 1968).
[21] P. VanHoof, Atomic Line List, http://www.pa.uky.edu/peter/atomic/.
[22] G. Herzberg, *Atomic Spectra and Atomic Structure* (Dover, New York, 1944).
[23] L. L. Lao, H. S. John, R. D. Stambaugh, A. G. Kellman, and W. Pfeiffer, Nucl. Fusion **25**, 1611 (1985).
[24] H. P. Summers, Atomic Data and Analysis Structure, http://adas.phys.strath.ac.uk.

Downloaded 22 Mar 2004 to 198.35.3.213. Redistribution subject to AIP license or copyright, see http://rsi.aip.org/rsi/copyright.jsp